SANDIA REPORT
SAND201X-XXXX
Unlimited Release
Printed September 2017

Visible Quantum Nanophotonics

Ganapathi S. Subramania, George T. Wang, Arthur J. Fischer, Jonathan J. Wierer, Jeffrey Y. Tsao, Daniel D. Koleske, Michael E. Coltrin, Sapan Agarwal, P. Duke Anderson and Ben Leung

Prepared by
Sandia National Laboratories
Albuquerque, New Mexico 87185 and Livermore, California 94550

Sandia National Laboratories is a multimission laboratory managed and operated by National Technology and Engineering Solutions of Sandia, LLC, a wholly owned subsidiary of Honeywell International, Inc., for the U.S. Department of Energy's National Nuclear Security Administration under contract DE-NA0003525.

Issued by Sandia National Laboratories, operated for the United States Department of Energy by National Technology and Engineering Solutions of Sandia, LLC.

Available to DOE and DOE contractors from
U.S. Department of Energy
Office of Scientific and Technical Information
P.O. Box 62
Oak Ridge, TN 37831

Telephone: (865) 576-8401
Facsimile: (865) 576-5728
E-Mail: reports@osti.gov
Online ordering: http://www.osti.gov/scitech

Available to the public from
U.S. Department of Commerce
National Technical Information Service
5301 Shawnee Rd
Alexandria, VA 22312

Telephone: (800) 553-6847
Facsimile: (703) 605-6900
E-Mail: orders@ntis.gov
Online order: https://classic.ntis.gov/help/order-methods/

SAND201X-XXXX
Printed September 2017
Unlimited Release

Visible Quantum Nanophotonics

Ganapathi S. Subramania , Jonathan J. Wierer, P. Duke Anderson
Semiconductor Materials and Device Sciences

George T. Wang, Daniel D. Koleske, Michael E. Coltrin, Ben Leung
Advanced Material Sciences

Arthur J. Fischer
Quantum Phenomena

Jeffrey Y. Tsao
Semiconductor and Optical Sciences

Sapan Agarwal
Assured Digital Syst & Comp

Sandia National Laboratories
P. O. Box 5800
Albuquerque, New Mexico 87185-MS1082

Abstract

The goal of this LDRD is to develop a quantum nanophotonics capability that will allow practical control over electron (hole) and photon confinement in more than one dimension. We plan to use quantum dots (QDs) to control electrons, and photonic crystals to control photons. InGaN QDs will be fabricated using quantum size control processes, and methods will be developed to add epitaxial layers for hole injection and surface passivation. We will also explore photonic crystal nanofabrication techniques using both additive and subtractive fabrication processes, which can tailor photonic crystal properties. These two efforts will be combined by incorporating the QDs into photonic crystal surface emitting lasers (PCSELs). Modeling will be performed using finite-different time-domain and gain analysis to optimize QD-PCSEL designs that balance laser performance with the ability to nano-fabricate structures. Finally, we will develop design rules for QD-PCSEL architectures, to understand their performance possibilities and limits.

ACKNOWLEDGMENTS

Authors would like to acknowledge Karen Cross , John Nogan, Denise Webb and Bill Ross for help in various aspects of nanofabrication, Anthony James for training student with e-beam lithography and Anthony Coley and Michael Smith on training of students and postdocs as well as help with laser spectroscopy.

TABLE OF CONTENTS

FIGURES

TABLES

No table of figures entries found.

EXECUTIVE SUMMARY

The goal of this LDRD is to develop a quantum nano photonics capability that will allow practical control over electron (hole) and photon confinement in more than one dimension. We plan to use quantum dots (QDs) to control electrons, and photonic crystals to control photons. InGaN QDs will be fabricated using quantum size control processes, and methods will be developed to add epitaxial layers for hole injection and surface passivation. We will also explore photonic crystal nanofabrication techniques using both additive and subtractive fabrication processes, which can tailor photonic crystal properties. These two efforts will be combined by incorporating the QDs into photonic crystal surface emitting lasers (PCSELs). Modeling will be performed using finite-different time-domain and gain analysis to optimize QD-PCSEL designs that balance laser performance with the ability to nano-fabricate structures. Finally, we will develop design rules for QD-PCSEL architectures, to understand their performance possibilities and limits.

NOMENCLATURE

Abbreviation	Definition
QD	Quantum Dots
QW	Quantum Wells
QSC-PEC	Quantum size controlled photoelectrochemical etch
QAP	Quasi-aperiodic
LED	Light emitting diodes
LD	Laser diodes
SOTA	State-of-the-art
PCE	Power conversion efficiencies
ICP	Inductively coupled plasma
MOCVD	Metal organic chemical vapor deposition
CCD	Charge-coupled device
PL	Photoluminescence
HBT	Hanbury Brown-Twiss
SPAD	Single-photon avalanche detector
TCSPC	Time-correlated single-photon correlator

1. INTRODUCTION

Applications for UV/visible lasers are many and include: free-space and underwater communications; solid-state lighting; bio-sensing/actuation/cide; free-space directed energy; quantum communication; and atomic clocks. All of these applications will benefit greatly from improvements in two key characteristics: electrical-to-optical energy-conversion efficiency, and directability. At one extreme, low-power applications need maximum useful work for minimum energy consumption; at the other extreme, high-power applications are typically heat-sink limited at the source and target-localization-limited at the sink.

The key to past improvements in efficiency and directionality has been simultaneous control over electron and photon confinement (in real space) and densities of states (in reciprocal space). Though past improvements have been revolutionary, practical devices use one-dimensional structures: quantum wells for control of electrons and Fabry-Perot-like cavities for control of photons. Even more revolutionary improvements are possible when control is extended to more than one dimension.

In this report, we describe a quantum nanophotonics based architecture in the visible frequency regime that enables practical control over electrons and photons in more than one dimension. In other words it is a regime when discrete quantum objects and quantum states (e.g., quantum dots) interact with high Q cavities and resonances (e.g., photonic crystals). The motivation for this work is that synergistic interaction between electrons and photons might lead to ultra-efficient light sources and lasers which in turn might lead to area-scaled ultra-high-power lasers (also interesting). There are some key challenges that need to be met : 1) creation of dense array of quantum dots (QDs) 2) optimization of the QDs interaction with the photonic crystals (PC) through precise spatial and spectral alignment. In this work we study this in a III-nitride system based on InGaN quantum wells (QW) on GaN epitaxial film. To create the QDs we use a top-down etch approach based on a quantum size controlled photoelectrochemical etch (QSC-PEC) technique to create deterministically placed single quantum dots from single quantum wells(SQW) or multiple QDs from multiple quantum wells (MQW). The photonic crystals designs are explored that optimize the interaction of such QDs to maximize the spontaneous emission enhancement as well as to optimize light extraction and far-field profile control. Fundamental understanding of this will create pathway for creating efficient room temperature single photon sources and for ultra-efficient lasers that can potentially be area scalable.

In the upcoming sections we will describe the motivation for using QDs as light source followed by top-down nanofabrication approach to creating QDs from planar films containing InGaN QWs . This will be followed by sections on study of deterministically placed single QDs and control farfield emission pattern using a quasi-aperiodic (QAP) III-nitride nanowire array PC respectively. In the final section we will provide a short summary and future outlook.

2. III-NITRIDE QUANTUM DOTS AS ACTIVE REGIONS FOR LEDS AND LASERS

III-nitride light-emitting diodes (LEDs) and laser diodes (LDs) are ultimately limited in performance due to parasitic Auger recombination. For LEDs, this results in poor efficiencies at high current densities while for LDs, the consequences are high thresholds and limited efficiencies. In this section we present arguments for III-nitride quantum dots (QDs) as active regions for both LEDs and LDs, to circumvent Auger recombination and achieve efficiencies at higher current densities that are not possible with quantum wells. QD-based LDs achieve gain and thresholds at lower carrier densities before Auger recombination becomes appreciable. QD-based LED achieve higher efficiencies at higher currents because of higher spontaneous emission rates and reduced Auger recombination. The technical challenge is to control the size distribution and volume of the QDs to realize these benefits. If constructed properly, III-nitride light-emitting devices with QD active regions have the potential to outperform quantum well light emitting devices, and enable an era of ultra-efficient solid-state lighting.

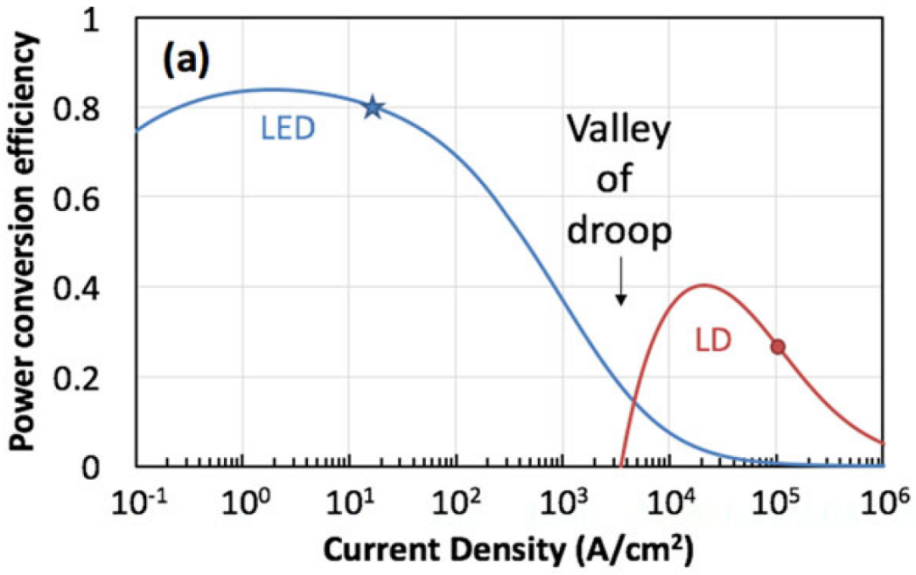

Figure 1. Plot of power conversion efficiency (PCE) vs. current density for a state-of-the-art (SOTA) LED and LD emitting at violet wavelengths.

III-nitride light-emitting diodes (LEDs) have achieved high peak power conversion efficiencies (PCEs) of ~ 84% [1] resulting in becoming cost competitive with traditional lighting technologies[2]. However, a phenomenon called "efficiency droop" where the radiative efficiency of III-nitride quantum well (QW) LEDs decreases with increased current[3-6] sets in due to Auger recombination, and consequently limits the peak PCE

to low current densities (< 10 A/cm^2). The most effective method, to date, to mitigate efficiency droop is to shift the onset to higher currents by lowering the carrier density at a particular operating current. For a fixed areal chip cost, LEDs operated at low current densities will typically produce fewer lumens per unit chip cost, hence there is tremendous economic incentive to mitigate Auger recombination and efficiency droop[7]. III-nitride laser diodes (LDs) are also gaining interest as an alternative source for SSL. In contrast to LEDs, LD operate under stimulated emission after lasing threshold, and parasitic recombination processes such as Auger are clamped at threshold. The result is III-nitride LDs have higher PCEs at much higher current densities than LEDs, and are a potential way to overcome efficiency droop[7]. Auger recombination not only limits LED performance, but also LD performance. This is illustrated in Figure 1 which shows PCE versus current density for a state-of-the-art (SOTA) LED, and SOTA LD both emitting at violet (405-415 nm) wavelengths. For LEDs, Auger recombination grows super-linearly with increased current density and dominates at high currents, relegating the peak PCE to low current densities (<10 A/cm^2). For LDs, Auger recombination becomes an appreciable fraction of the total current near threshold, causing a high threshold current density and high parasitic resistive losses, which in turn limits the peak PCEs of the LD. Between the PCE peaks is the valley of droop at mid-range current densities where both emitters are inefficient.

For both LD and LEDs, we need to improve efficiencies at the valley of droop or higher currents to further advance SSL. Transformational methods will need to be found to address the limitations imposed by Auger recombination. One possible approach is to use a new type of active region in III-nitrides to achieve drastic reductions in threshold carrier densities and increases in spontaneous emission rates. Such improvements are essential to improve higher current performance in both LEDs and LDs. It has been recognized for some time that quantum dots (QDs) have benefits over QWs. For LDs, QDs can be used to achieve lower threshold currents due to higher gain and lower threshold carrier densities. For LEDs, the QDs higher spontaneous emission will counteract Auger recombination, and additionally there is experimental and theoretical evidence that QDs should have suppressed or completely inhibited Auger recombination. QD active regions in LDs and LEDs could lead to more efficient sources in the valley of the droop and higher currents.

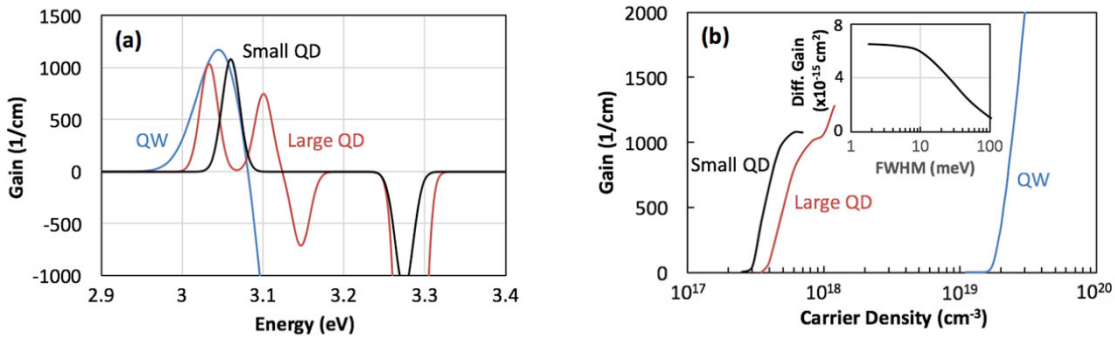

Figure 2. a) Plot of gain spectra for a single QW at N = 2.5×1019 cm−3 (blue line), a layer of large QDs at N = 9×1017 cm−3 (red line), and a layer

of small QDs at N = 7×1017 cm−3 (black line). b) peak gain vs. carrier density for a single QW, a layer of large QDs, and layer of small QDs. Inset plots the differential gain of the small QDs vs. the full-width at half maximum (FWHM) of the inhomogeneous broadening energy.

Below, we will explore QDs as the active layer for LEDS and LDs. First, we investigate QDs as active layers for LDs to reduce threshold and peak PCE current densities. A properly constructed InGaN QD active layer avoids appreciable Auger recombination, and, with high enough differential gain greatly reduces the transparency carrier density. Second, we investigate InGaN QDs in LEDs to overcome efficiency droop. Properly formed InGaN QDs leads to higher spontaneous emission and lower Auger recombination

To illustrate we compare the gain of a QD and QW active layer. Figure 2a shows the gain spectra versus energy for a single QW and single layers of QDs at carrier densities greater than N_{th}. Two different sizes of QDs are investigated, labeled small (~4-5nm) and large (~9-10nm). For the QWs and QDs the homogeneous broadening is 25 meV , and the inhomogeneous broadening for the QDs is 5 meV. While this inhomogeneous broadening is small, we will show it is necessary to achieve the ultimate improvement in threshold currents and PCE. The density of states for the QDs results in narrower gain spectra. For the large QDs the gain is shared with the many quantum states at multiple energies, while for the small QDs, the second energy transition is further away in energy and most of the carriers and gain is present in the lowest energy transition at the given carrier density. QD has a profound effect on G_0 (differential gain) and N_{tr} (transparency concentration) resulting in a lower threshold carrier density. Figure 2a shows the peak gain of a single QWand single layers of QDs versus carrier density.

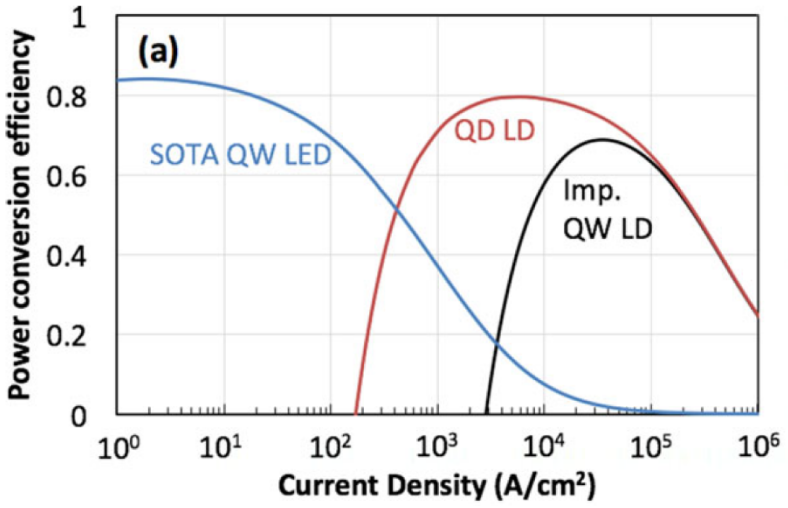

Figure 3. Plot of power conversion efficiency vs. current density of a state-of-the-art (SOTA), QW-based LED (blue line), an improved QW-based LD (black line), and a QD-based LD (red line). The QD LD has

extremely low threshold currents and peak efficiencies that rival the QW-based LED.

The QD layers have nearly two orders of magnitude lower N_{tr} than the QW. While the large QDs have low N_{tr}, the G_0 is less than the small QDs because of the additional

quantum states. To illustrate how dramatically different N_{th} and G_0 are, if we assume a threshold modal gain of 1000 cm−1, the QW would have $N_{th} = 2.4\times10^{19}$ cm^{-3} and $G_0 = 1.5\times10-16$cm^2, and the QD would have $N_{th} = 5.5\times10^{17}$ cm^{-3} and $G_0 = 6.5\times10^{-15}$cm^2. Therefore, we should expect a large decrease in threshold currents for QDs layers. It should be noted that the QDs saturate due to the limited number of quantum states. Therefore, to achieve enough gain either more than one QD layer or a larger QD density is required. The large QDs exhibit a saturation, followed by an increase in gain caused by the filling of the second favorable energy transition.

Up till now we have only considered low (5 meV) inhomogeneous broadening. The impact on differential gain on the full-width at half-maximum (FHWM) of the inhomogeneous broadening for the small quantum dots is shown in the inset of Figure 2b. As the FWHM increases the differential gain decreases. There is steep drop-off in differential gain at ~10 meV, and the differential gain at 5 meV is 7 times larger than at 100 meV. This translates into a 7 times difference in the threshold carrier density.

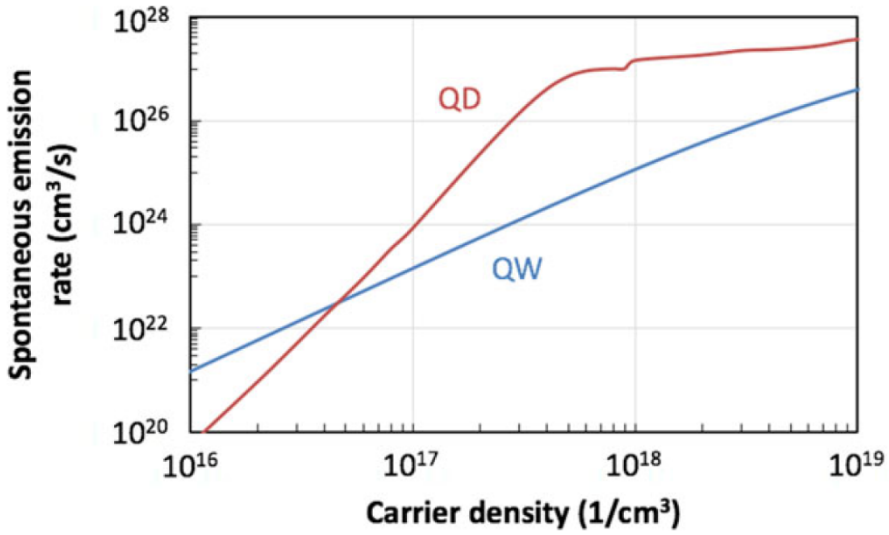

This plot illustrates how critical it is to control the inhomogeneous broadening within

Figure 4. Plot of (a) spontaneous emission rate vs. carrier density for a QW (blue) and QD (red) active region. The QD active layer has higher spontaneous emission rates over the carrier densities of interest. The kink in the curve at ~1×10^{18} cm^{-3} is the onset of carrier filling in the second allowed transition

the QD layers. The lower threshold carrier densities of the QDs have a big impact on the PCE. Figure 3 shows the PCE versus current density for a QD-based LD with 6

layers of small QDs at a density of ~7.2×10^{10} cm^2. The SOTA QW-based LED and improved QW-based LD are included for comparison. The threshold current density of the QD LD is ~170 A/cm^2 , over an order of magnitude lower than the improved QW-based LD. The peak PCE is ~80% at ~5.7 kA/cm^2 which is a much lower current density for peak PCE and rivals the peak PCE of the LED. The large reduction of threshold currents goes a long way to filling the valley of droop.

It is also interesting to compare the PCE of the SOTA QW-based LED[1] to a QD-based LED only considering the small QDs. Figure 4 shows the total spontaneous emission rate (R_{sp}) for the QWs and QDs with increasing carrier density. The QDs have higher spontaneous emission at carrier densities of 10^{16}–10^{19} cm^{-3}. The QDs have a more rapid increase in spontaneous emission at low carrier densities with an expected saturation at ~5×10^{17}, similar to the gain. However, the LEDs can operate at higher carrier densities than LDs, and at ~1×10^{18} cm^{-3} there is a kink in the spontaneous emission curve due to carriers populating the second energy transition. This second transition is not considered as a parasitic recombination path because the produced photons can be used to pump phosphors, so it is included in the total spontaneous emission rate.

We can now explore how the higher R^t_{sp} for QDs and different Auger recombination rates impact PCE. Figure 5 shows the PCE versus current density for QD-based LEDs

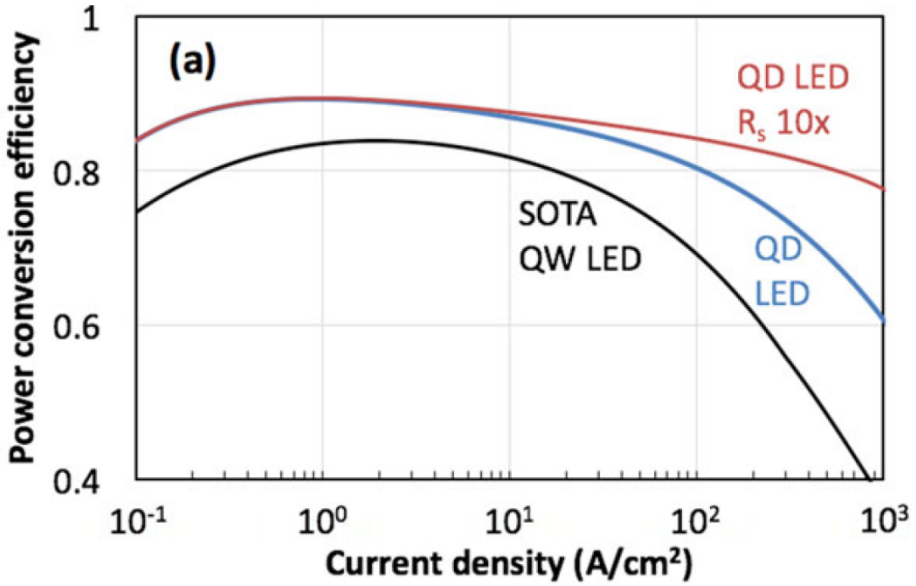

with various rates and the SOTA QW-based LED. The QD based LEDs use the

Figure 5. Plot of power conversion efficiency vs. current density for a state-of-the-art (SOTA) QW LED (black line), a QD LED with increased spontaneous emission rate (QD LED, blue line), and a QD LED with an additional decrease in series resistance (QD LED Rs 10x, red line). The QD LEDs have improved efficiencies.

calculated R^t_{sp} while the SOTA QW based LED uses the fitted BN^2. All the QD based LEDs have higher PCE, because of the higher spontaneous emission rate. For the QD LED (blue line) the C_0 coefficient is held constant at 10−30 cm^6/s, or raised and lowered by 10 times, and surprisingly all three Auger recombination rates produce the same PCE curve. This shows the high R^t_{sp} diminishes the effect of the Auger recombination rate. With high R^t_{sp}, the decrease in PCE at high current densities is now dominated by series resistance. The highest PCE curve (red line) includes an additional reduction in series resistance by 10 times. This analysis shows that if such QDs LEDs can be realized, series resistance will become the limiting factor in PCE. The improvements in PCE will result in higher efficiency pc-LEDs. This work was published in reference [8] .

The most successful method to produce InGaN QDs is Stranski-Krastanov (SK) growth. This synthesis method can produce QDs with enough gain for LD operation, however the inhomogeneous broadening is large (~50-100 meV) and QD sizes can be large (up to 40 nm width). Additionally, the QD densities are modest at ~$3\text{-}4\times10^{10}$ cm^2. One potential method to create QDs with low inhomogeneous broadening, smaller QD sizes, and higher QD densities is quantum-sized controlled photoelectrochemical etching (QSC-PEC). In the following sections we will discuss III-nitride QDs created using this approach including the challenges and their optical properties.

3. TOP-DOWN FABRICATION OF III-NITRIDE NANOPHOTONIC STRUCTURES WITH QSC-PEC

Sandia has recently developed a new two-step top-down fabrication approach for the realization of high-quality III-nitride semiconductor nanowires[9-10] which are of significant interest for optoelectronic and other applications. This approach combines an inductively coupled plasma (ICP) dry etch with a crystallographically anisotropic KOH-based wet etch. Due to the unique characteristics of this wet etch for GaN, highly vertical nano- and micro-structures with controlled dimensions and positioning can be realized starting from high-quality epitaxial GaN material. Here, we further investigated extending this top-down approach towards our goal of realizing quantum nanophotonic structures. In particular, we hope to realize high-gain photonic structures with quantum-dot active regions. Thus, our approach is to realize high-quality, vertical nanostructures which will contain the QDs and can be arranged in photonic crystal designs. Recent investigations into the dry and wet etch mechanisms of our technique have allowed us to understand the conditions leading to specific nanostructure cross-sections and morphologies, including rectangular and annular[11-12] which have important implications for their optical properties. Here, electron-beam lithography (EBL) was used to define Ni stripes oriented along the [11-20] a-axis and [1-100] m-axis directions on a (0001) c-plane GaN epilayer grown on c plane sapphire substrate by metal-organic chemical vapor deposition (MOCVD). Following our top-down approach, well-defined GaN nanosheets, or nanowalls, with vertical sidewalls were successfully realized, as shown in Figures 6(a) and 6(b). The optical characteristics of the nanosheets were studied by room-temperature micro-photoluminescence experiments using a 266 nm pulsed Nd:YAG pump laser. For nanosheets with smooth m plane sidewalls, shown in Figure 6(c), luminescence coupled to cavity modes can be observed. For nanosheets with rougher a plane sidewalls, these cavity modes are not observed, underlying the importance of surface morphology on optical properties.

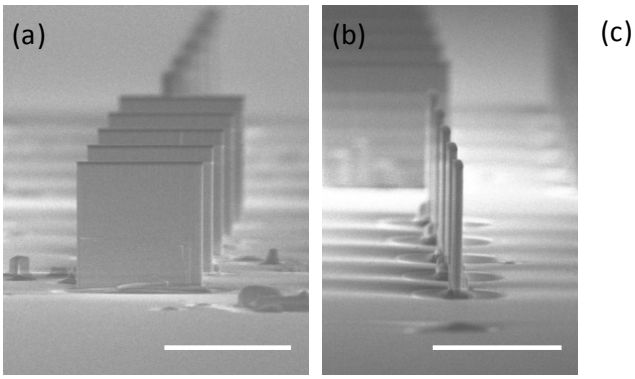

Figure 6. (a) and (b) Scanning electron micrograph (SEM) images of top-down fabricated GaN nanosheets with m-plane sidewalls. (c) Room temperature micro-PL of a nanosheet with m-plane sidewalls, showing luminescence coupled with cavity modes.

Other types of crystallographically selective wet etches for GaN would also be of great interest for nanophotonic and nanoelectronics structures. One example of relevance we have demonstrated, shown in Figure 7, is an inverse tapered etch. This unique morphology can lead to significantly enhanced optical confinement by separation of the active or gain region from the substrate, and can potentially be used in our photonic structure designs. Specifically, the need for complex and difficult-to-realize mirrors, such as lattice-mismatched AlGaN/GaN distributed Bragg reflectors, could potentially be avoided using this type of architecture.

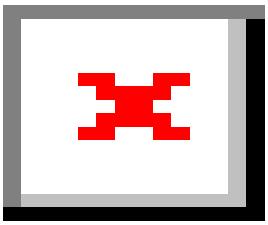

Figure 7. Inverse tapered GaN nanowires fabricated by our two-step top-down approach.

To realize InGaN-based quantum dot active regions, we utilize a recent, Sandia-demonstrated approach known as quantum-size controlled photoelectrochemical etching. In this method, quantum size effects themselves can be harnessed to precisely control nanofabrication. The principle is summarized as follows: as a nanostructure shrinks due to light-induced photoetching, its bandgap increases due to quantum confinement effects. It will thus eventually cease to absorb light and stop etching when its bandgap exceeds the energy of the light. QSC-PEC etching thus works on a bandgap selective mechanism that self-terminates etching at a wavelength-determined size. This is fundamentally different from conventional methods that attempt to control size via timing of etch or growth rates and that are ill-suited for precise control at the sub-10 nm size regime. Also, conventional self-assembled growth of QDs requires compressively strained QDs, which greatly limits possible QD material and substrate combinations.

While single-layer InGaN QDs have been demonstrated by this approach[13-14] multiple layers of QDs are desired to increase the gain needed for QD-based laser structures. To this end, we have grown InGaN/GaN multiple quantum well structures with the goal of turning the quantum wells into multiple layers of quantum dots via QSC-PEC etching. PEC etching was performed on this sample at an etch wavelength of 420 nm in 0.2M H_2SO_4 for 45 minutes. The results show that all five InGaN quantum wells were etched (Figure 8), with QDs visible along with large etched-away void regions. PL experiments show a blue shift in the PL emission of the PEC-etched MQW,

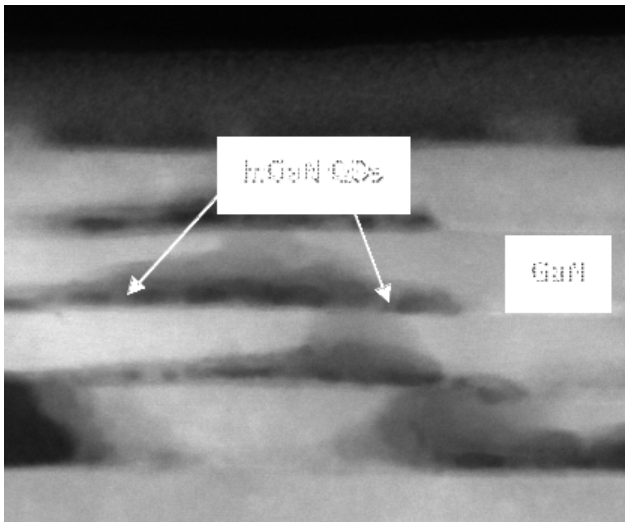

Figure 8. Five InGaN/GaN MQW heterostructure after QSC-PEC etching, showing formation of multiple layers of InGaN QDs

supporting the formation of QDs. However, the PL intensity of the etched QD sample is only slightly higher than that from an etched single capped QW InGaN/GaN sample, rather than the expected ~five times increase due to the five times increase in

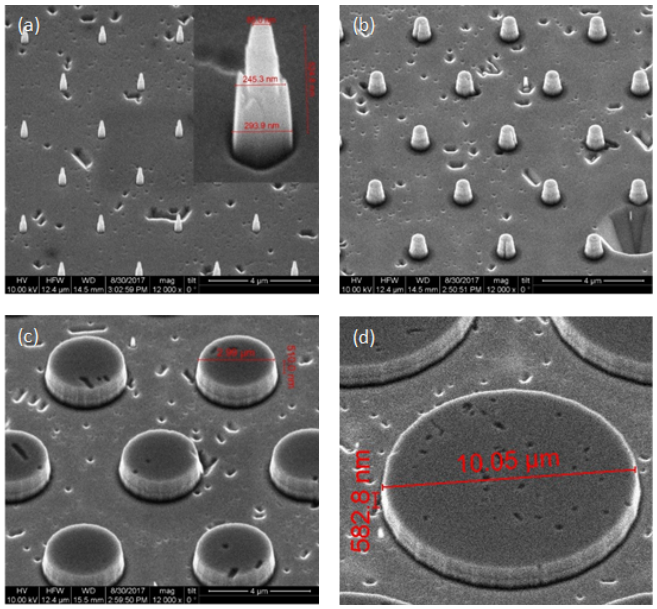

numbers of QWs. A possible reason is that the QD density per etched QW is lower

Figure 9. (a)-(d) SEM images of patterned and etched pillars of varying dimensions, from ~250 nm to 10 µm, from a five InGaN/GaN MQWs heterostructure.

than that for a single QW, due to the requirement of needing to etch through multiple GaN barriers, which may lower yield.

To address this, we have designed, patterned, and etched nano- and micro-pillar structures from a InGaN/GaN MQW structure which will help us optimize the PEC etch conditions to maximize QD density in the structures, as shown in Figure 9. As the QWs are exposed at the pillar sidewalls, this will avoid the need to etch through the GaN barriers, which are above the bandgap of laser light used for etching, and allow for the InGaN layers to be etched directly and laterally. One open question that future PEC experiments of these etched MQW pillars will help answer is how the QD density of the etched layer may be affected by the MQW structure and the pillar diameter. In some cases, a minimal density of QDs may be desired, e.g. for single photon emitters.

4. DETERMINISTIC PLACEMENT OF QUANTUM-SIZE CONTROLLED QUANTUM DOTS

While multiple QDs can be important as an active source for light emission single quantum dots can also be important especially for quantum sources such as single photon sources. The high exciton binding energy of III-nitrides (~ 30meV) enables the possibility room temperature single photon sources. Single photon sources are light sources where photons are emitted one at a time i.e. as opposed to being emitted in a bunch like in thermal sources. This property referred to as photon anti-bunching[15-22] is a key measure of the single photon sources. One main challenge has been deterministic placement of such quantum dots to enable coupling to optical cavity modes to enhance single photon emission rates as well as extraction into free space. Below we discuss our approach on fabrication of deterministically patterned QDs using electron beam lithography and their optical properties.

QDs due to their three dimensional confinement possess discrete atomic-like energy levels are artificial atoms there by providing unique advantages. Owing to their size, which is on the order of a semiconductor's exciton Bohr radius, quantum-size effects grow prominent in QD nanostructures[23] . Consequently, QDs' discrete energy levels determine their absorption/emission spectra making them highly suitable for single photon sources.

Several nanofabrication approaches currently used for producing semiconductor QDs, rely upon solution-based synthesis techniques[19, 22, 24-25] that are mostly suitable for incorporation on the surface of photonic structures. In order to introduce QDs inside the semiconductor so as to be more compatible with semiconductor based nanophotonic applications[19, 26-30] one requires either bottom-up self-assembly or top-down synthesis. However, two main challenges encountered when using either synthesis approach are deterministic placement and size control l[19] . Bottom-up growth techniques such as the Stranksi-Krastanov (SK) [31] growth result in III-nitride QDs with superior surface quality due to the natural in-situ passivation provided by the subsequently grown semiconductor layers. Nevertheless the self-assembled nature of such QDs result in large uncertainty in QD location and significant fluctuations in QD size. As a result, integrating bottom-up growth techniques with nanophotonic designs, such as high-quality factor (Q-factor) microcavities, often involve complex alignment procedures and can face low device yields[19, 32-34]. As described in the previous section we have pursued the top-down wet-etch approach[13-14] for the fabrication of III-nitride QDs using QSC-PEC etching. This approach is more amenable to subsequent photonic device integration and higher device yields.

To fabricate a deterministically placed quantum dot we start with a top-down nanowire fabrication which is shown schematically in Figure 10. We begin by spinning on polymethylmethacrylate (PMMA) resist and patterning a series of holes using EBL. The pattern consists of a square array of holes, approximately 100 – 200 nm in diameter with 1 μm and 2 μm spacing. After developing, next the openings are filled with approximately 30 nm of Ni via electron beam evaporation. Ni dots are formed by ultrasonicating the sample in an acetone bath. This is followed by an inductively coupled plasma (ICP) etch utilizing a Cl_2/BCl_3-based chemistry, with the

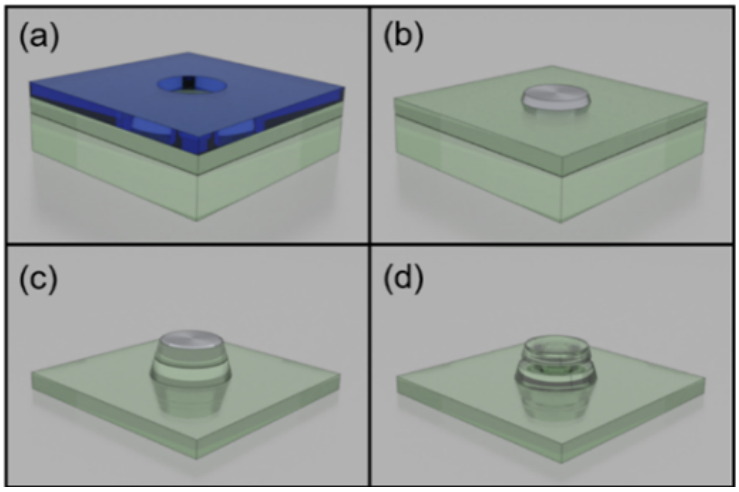

Figure 10. Nanofabrication schematic a) EBL patterning b) Ni deposition c) Lift-off d) PEC etch.

Ni islands functioning as a hard mask. The remaining Ni is removed in a dilute solution of H_2SO_4 after the Cl_2/BCl_3-based dry etch. Next, we suspend approximately half of our patterned sample is suspend in the PEC etch solution as shown in Figure 11. Partial sample immersion permits the comparison of unetched regions (QWs) to QSC-PEC etched regions (QDs) later in our study. In the setup, a III-nitride sample is immersed in an electrolyte solution. Here, we select ~ 0.2 M H_2SO_4 as our aqueous electrolyte, allowing us to avoid material etching in the absence of light. A cathodic In electrode is bonded to the III-nitride sample while an anodic Pt electrode is suspended in the electrolyte solution. During the PEC etch, electron-hole pairs are generated using a relatively narrow linewidth laser ($\Delta\lambda_{FWHM}$ ~ 1 nm). Due to the applied electric potential, photoexcited holes are attracted to the material surface where they contribute to surface oxidation. As the size of the QW region reduces, quantum size

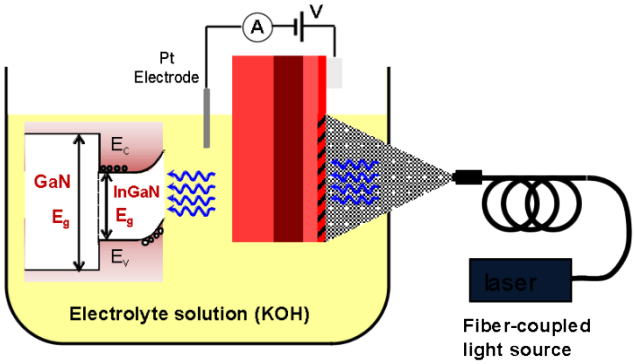

effects emerge and begin to increase the electronic bandgap of the structure.

Figure 11. Schematic of QSC-PEC etch process

Eventually, a QD is formed and the bandgap becomes too large for light to be absorbed, thereby self-terminating the etch process in the III-nitride sample. Thus, properly selected narrowband light can be absorbed by large nanostructures but not by smaller nanostructures. In this manner, the size of the resulting nanostructures is determined by the wavelength of the incident light. We perform the QSC-PEC etch using a photoexcitation source consists of a frequency-doubled Ti:Sapphire laser with a 82 MHz repetition rate and a 2 ps pulse width, producing an average power of 30 mW at a wavelength of 420 nm. The laser light is coupled to an optical fiber and sent to the etch setup. The excitation wavelength corresponds to an energy lower than the bandgap of GaN but above that of the InGaN QW, enabling selective PEC etching of the QW. The QSC-PEC etch is typically performed for 90 minutes. At this point in the etch process, the etch current converged to a few nA, indicating that no appreciable etching was occurring and that the etch process had terminated. Figure 12a shows a

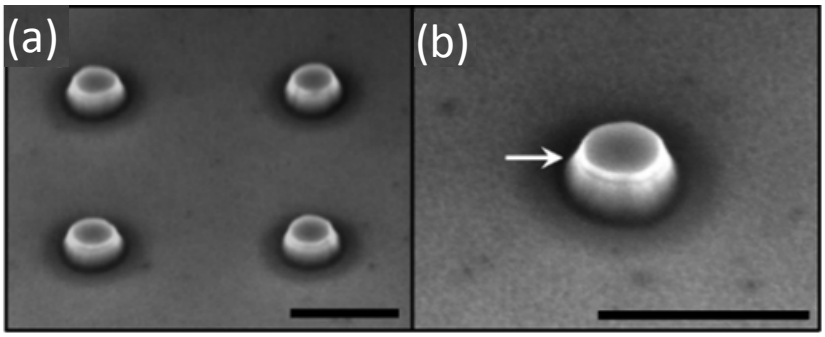

scanning electron micrograph (SEM) of a fabricated nanowire array. In the figure, nanowires have nominal diameters of 200 nm and are separated by 1 μm. Figure 12b shows a magnified SEM of a single QSC-PEC etched nanowire.

Figure 12. a) SEM images of fabricated nanowire array. b) Magnified image of nanowire; white arrow indicates etched region.

We performed low-temperature mirco-photoluminescence (μ-PL) measurements of etched nanowires to obtain optical response of the nanowires. The device was housed in a cryostation that was nominally cooled to a temperature, T = 10 K. The sample was optically excited (using the same tunable laser) at a wavelength of 375 nm and average power of 5 μW. A 50X near-UV Mitutoyo objective focused the laser to a spot size of nearly 1 μm^2 on the sample. The device was imaged using the same objective and directed into a 0.3 meter focal length spectrometer with an attached liquid N_2 cooled charge-coupled device (CCD) camera.

Emission from a QSC-PEC etched nanowire with a diameter of 200 nm is shown in Figure 13a . Three peaks are observed at wavelengths of 411 nm, 413 nm and 418nm, with the third peak being most prominent, exhibiting a large intensity 4-5 times larger than the other two peaks (after background PL correction). The narrow linewidths associated with the peaks ($\Delta\lambda_{FWHM} < 0.3$ nm) show that they are QD-like emission signatures. However, following QSC-PEC etching, there is a significant blue shift in the emission wavelength ($\lambda \sim 415$ nm) from the original single QW had a PL emission wavelength of 450 nm (data not shown), corresponding to an In fraction of nearly 15%.. When moving from a QW to a QD, the emission blue shift results from

an energy level increase due to in-creased carrier confinement. This is the fundamental principle behind QD formation using QCS-PEC etching[13]. Multiple emission peaks, however, suggests the presence of multiple QDs within a single nanowire. Likely reason behind this could be due to the fact that the nanowire diameter (~ 200 nm) is relatively large compared to the GaN capping layer (~ 30 nm). Consequently, the lateral PEC etch, which is the desired mechanism, competes with the vertical etching of nitride material that takes place through unavoidable threading dislocation defects in the GaN capping layer. These competing PEC etch directions may result in the formation of multiple QDs in a single nanowire. Furthermore, the

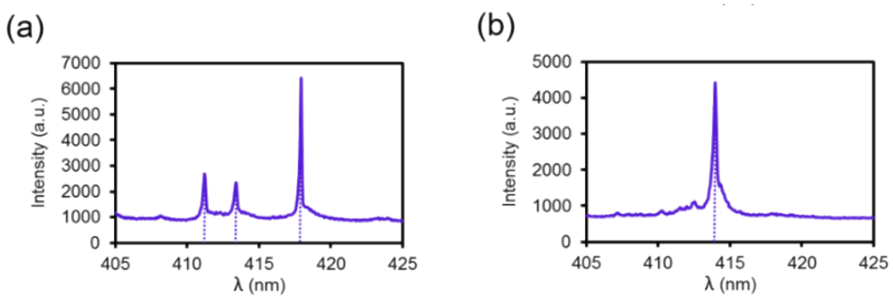

spacing between neighboring nanowires (1 μm) is comparable to the spot-size diameter of our focused pump beam. Consequently, misalignment or slight defocusing may contribute to pumping more than one nanowire simultaneously.

Figure 13. a) PEC etched 200nm diameter nanowire. b) PEC etched 100nm nanowire.

We fabricated QSC-PEC etched nanowire arrays featuring smaller diameters (~ 100 nm) and greater neighbor-to-neighbor spacing (2 μm) to address the above issues. Figure 13b shows the low-temperature μ-PL associated with one such nanowire. In the figure, a single sharp peak with a narrow peak linewidth ($\Delta\lambda_{FWHM}$ ~ 0.3 nm) is observed at a wavelength of 414 nm. This peak is highly suggestive of single QD formation. Deterministic placement of the isolated QD location is achieved by two criteria namely, the vertical location of the QW in the original epitaxial structure (determined during growth) and the cross-sectional location of the nanowire (determined during patterning). Therefore, careful selection of these parameters, in addition to the etch-assisted laser wavelength, offers a unique opportunity in spatially and spectrally coupling QSC-PEC etched QDs to pre-patterned PhC cavities. For instance, L1 PhC cavities are an immediately attractive candidate, containing defect surface areas comparable with the nanowire diameters studied here. Further, our approach is top-down and highly sensitive to material absorption windows, allowing preferential etching of InGaN structures. Finally, the knowledge of position of resonances preceding QSC-PEC etching provides direction in selecting the wavelength necessary for spectrally coupling the QD to a resonant cavity mode.

The motivation for creating site-controllable quantum dots is for subsequent utilization in a quantum light source. In order to study this, we investigate the photon statistics of isolated QDs using a Hanbury-Brown and Twiss (HBT) setup, illustrated in Figure 14a. The setup consists of light coming from a low-temperature QD PL that is split into two paths using a 50/50 beamsplitter. Light from each path is optically focused

onto two, single-photon avalanche detectors (SPADs). The signal from each detector is then fed into a time-correlated single photon counting (TCSPC) module. Figure 14b

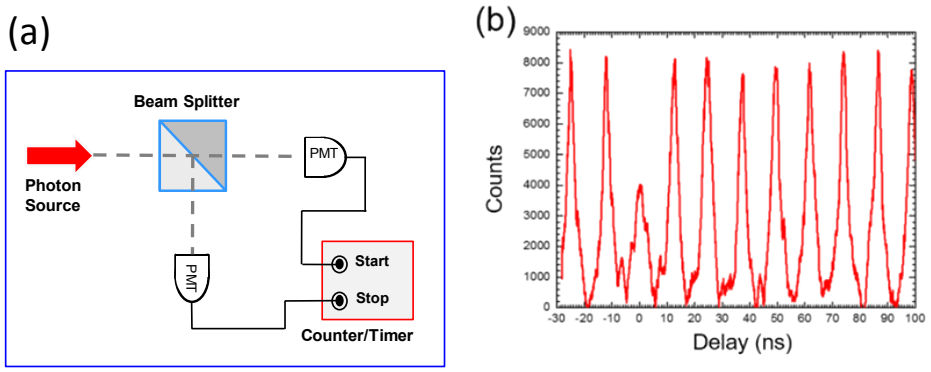

Figure 14. a) Schematic of the HBT setup. b) Second order photon correlation g^2.

shows the second-order cross-correlation ($g^2(0)$) of low-temperature QD PL collected under pulsed operation. At t=0, there is a large reduction in photon counts, yielding a $g^2(0) \sim 0.5$. This indicates lowered probability of a second photon arriving at the detector at the same time when one photon is already detected. The ideal value is ~0. This value for a typical laser is ~ 1 indicating random photon emission while ~2 for bunched photon emission as in thermal sources. The g^2 result clearly indicates photon anti-bunching, a non-classical behavior associated with single photon emission. However factors such as low light-collection and potential background emission from defect GaN sites leads to large noise in the measurement. Incorporating QSC-PEC etched QDs into properly designed PhC defect cavities will enable improvement of light-collection and emission rate enhancement, through the Purcell effect. Improving the emission signatures of QSC-PEC etched QDs using such structures could greatly improve signal-to-noise ratios and enable the development of room-temperature, single photon sources. This work was published in reference [35].

5. TAILORING EMISSION UNIFORMITY USING QUASI-APERIODIC DESIGN IN NANOWIRE ARRAYS

As described in section 2 QDs can be used to achieve lower threshold currents due to higher gain and lower threshold carrier densities can therefore be better emitters compared to planar QWs. However, creation of QDs even in high density scenario invariably reduces the emitter volume compare to a QW based emitter design. So the gain achieved through QD formation is somewhat reduced because of this. Photonic structures typically PCs and PC cavities can plays significant role in tailoring emission in nanoemitter systems[36-45]. They can achieve this by capitalizing on enhanced emission rates due to density of states enhancements and/or Purcell effect. The former is typically observed at the band edges where group velocity is small enabling longer interaction time with the gain media (in this case, QDs) resulting in enhanced emission. PCs also enable to tailor the dispersion (frequency vs. wavevector) which can provide additional functionality such emission directionality and far field mode profile. In this section we will discuss how one can control far field emission profile by modifying the emitter position inside a sub-lattice of a periodic structure.

The typical goal is to utilize the enhanced photonic density of states especially at the band edges of a PC (near the Gamma point for normal emission) to enhance emission rate so as to achieve lasing at low threshold. However, in many cases the symmetry that is inherent in the PC results in a far-field emission patterns that is non-uniform with a ring like pattern. Such symmetry arising from circular holes in PC can be broken by changing the shape of the hole into something of lower symmetry such as a triangle. However, the fabrication methods such as either bottom-up through epitaxial growth or top-down using etching make it difficult to arbitrarily change the shapes of nanowires due to growth considerations and etch-plane competition. Consequently, new methods for improving the far-field uniformity of uncoupled modes in III-nitride nanowire systems are of interest for a variety of lighting and lasing applications. An alternative approach to breaking the symmetry is to change the emitter position within a photonic crystal supercell (2x2) –referred to here as quasi-aperiodic(QAP) array, thereby linearizing the photonic bandstructure near the Γ-point thus greatly improving emitted far-field uniformity. In quasi-aperiodic arrays, symmetry is broken by introducing asymmetry on a small scale and repeating the small-scale asymmetry on a larger scale. In our theoretical work, we predicted that quasi-aperiodic arrays could be leveraged to improve far-field emission uniformity without sacrificing broad band emission[46].

In this section we experimentally demonstrate the tailoring of emission using quasi-aperiodic nanowire arrays. Beginning with a III-nitride epitaxial structure we fabricate the structure using a top-down approach. We also fabricate simple periodic arrays, consisting of a square array of cylindrical nanowires as a reference for comparison of optical response with the quasi-aperiodic array. The two structures are characterized using room-temperature micro-photoluminescence (μ-PL) measurements which exhibit optical resonances. The resonance associated with the periodic array is shown to be much sharper than the quasi-aperiodic array, but produces a donut-like beam in

the far-field. On the other hand, the resonance associated with the quasi-aperiodic array is much broader, but produces a more uniform far-field emission pattern.

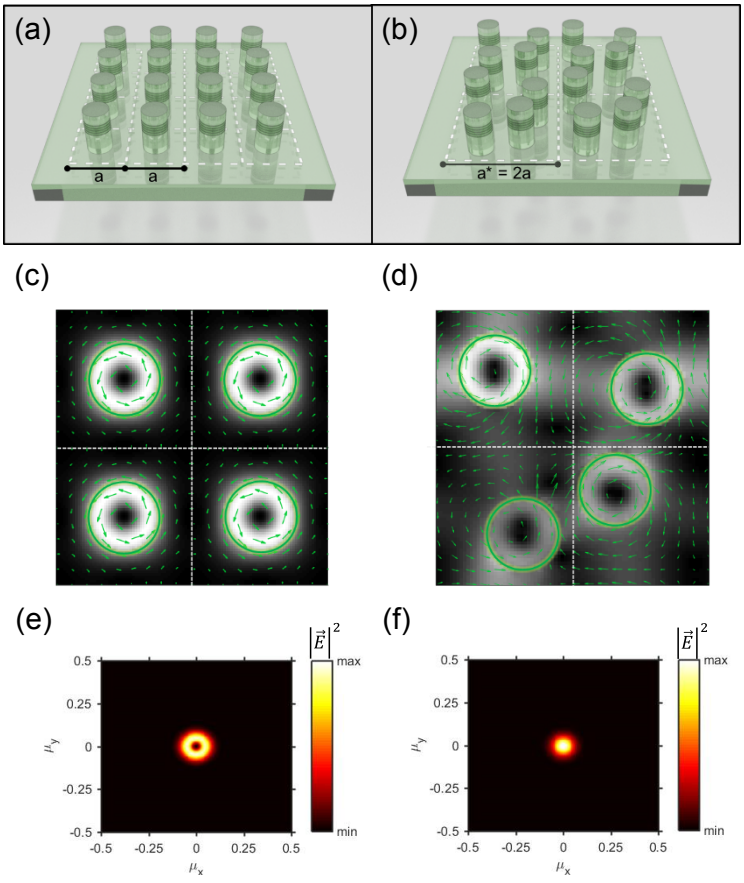

Figure 15. a) Schematic of periodic nanowire array. b) quasi-aperiodic array. c) and d) corresponding simulated in-plane electric field plots. e) and f) simulated far-field transmission.

We begin by considering the III-nitride system of a simple periodic array shown in Figure 15a. Each nanowire is composed of GaN containing five axial InGaN quantum wells. The lattice spacing is a, the rod height is h, and the nanowire radius is *r*. For the structures studied here the lattice constant *'a'* ranges from 240 nm – 280 nm, with *r/a* = 0.167 - 0.25 and *h* = 600 nm. The selection of these lattice parameters aligns a series of uncoupled, guided resonance modes within the emission bandwidth of the InGaN multiple quantum wells (MQWs). Figure 15b shows a quasi-aperiodic array wherein the dashed white lines indicate the boundaries of four complex unit cells, each containing four nanowires. Each complex unit cell in the quasi-aperiodic array is asymmetric, but the overall structure remains periodic on a larger scale. The nanowire height and radius are the same as for the simple periodic array, and the lattice constant of the complex unit cell is double that of the simple periodic array.

We use the top-down fabrication approach outlined in Figure 16. The method, developed in recent works, utilizes a combination of dry and wet etches to create an array of highly anisotropic nanowires[36]. We begin device fabrication by spinning

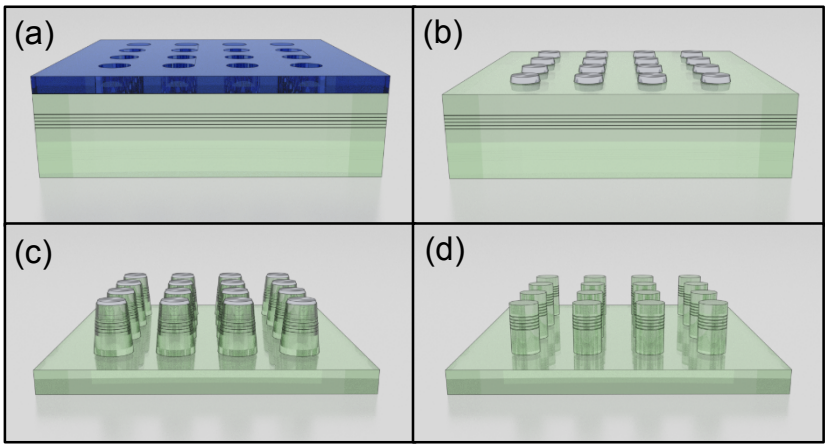

Figure 16. Schematic of device fabrication procedure: (a) EBL patterning of PMMA (b) Ni deposition followed by liftoff (c) Cl-based dry etch (d) KOH-based wet etch followed by H_2SO_4–based Ni removal.

Polymethyl methacrylate (PMMA) resist onto our sample and patterning an array of holes using electron beam lithography (EBL). Following development, the patterned holes are filled with Ni in an electron beam evaporator. Next, Ni islands are formed via lift-off in an acetone bath. Lift-off is followed with an inductively coupled plasma (ICP) etch, utilizing a Cl_2/BCl_3-based etch chemistry. The Ni islands function as a hard mask during the dry etch, leading to the formation of tapered nanowires. To improve nanowire anisotropy, the devices are immersed in a KOH-based solution at an elevated temperature. Finally, the remaining Ni is removed using H_2SO_4. Figure 17a and 17b show scanning electron micrographs (SEMs) for fabricated simple periodic and quasi-aperiodic nanowire arrays respectively8. Insets show top views of the complex unit cells in each respective structure. SEMs reveal cylindrical nanowires with smooth vertical sidewalls. The combination of a dry etch followed by a wet etch results in near atomically smooth sidewalls, effectively lowering non-radiative recombination. Typical device size was 20 μm x 20 μm. However, since this process results in etch termination at atomic planes[36], it is inherently difficult to arbitrarily change the shape of nanowires using this method. Consequently, in order to break field symmetry, it grows important to instead change the position of the nanowires using a supercell, as show in the inset of Figure 16b.

We optically characterized the fabricated devices at room-temperature using an ultraviolet micro-photoluminescence (μ-PL) setup. Our excitation source was a quadrupled Nd:YAG laser with a peak emission wavelength of 266 nm, a 10 kHz repetition rate and pulse lengths of ~ 500 ps. The laser's peak power density was adjusted using a tunable neutral density filter. A 50X Mitutoyo deep-UV objective

focused the laser to a spot size of nearly 5 μm onto the sample. Device photoluminescence was collected using the same objective, and divided into two separate paths using a 50/50 beamsplitter. The first path was used to image the

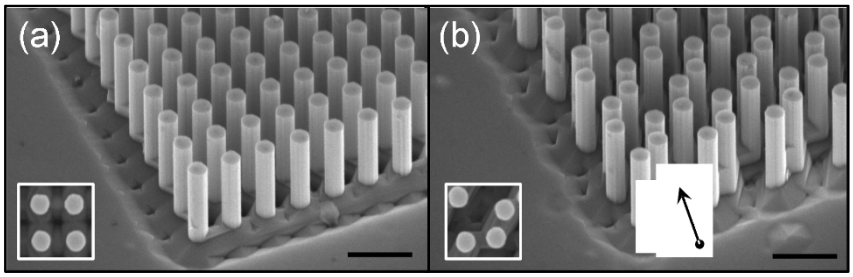

fabricated devices while the second path was directed into a 300 mm spectrometer and liquid N_2 cooled CCD camera for spectrum analysis.

Figure 17. SEMs for a (a) simple periodic and (b) quasi-aperiodic device. Insets show top views of complex unit cells in each structure. Black markers indicate a physical length of 500 nm. Black arrows indicate areas where nanowire bases are connected in the quasi-aperiodic array.

Figure 17 shows the optical response of a simple periodic (black) and a quasi-aperiodic (purple) structure to an optical pump as described above. The simple periodic structure exhibits a resonance at $\lambda \sim 410$ nm, corresponding to the gain window of the InGaN underlayer, and exhibits a quality factor (Q) of 390. On the other hand, the quasi-aperiodic resonance is red-shifted towards peak MQW emission ($\lambda \sim 440$ nm) and is broader with a much lower quality factor ($Q \sim 40$). The emission wavelength of the simple periodic array corresponds to a reduced frequency of $a/\lambda = 0.585$ (assuming a = 240 nm). Similarly, the emission wavelength of the quasi-aperiodic resonance corresponds to a reduced frequency of $a/\lambda = 0.545$ (assuming a = 240 nm, where $a^* = 2a = 480$ nm).

The significant difference in quality factors arises from the symmetries of the optical modes supported in each structure. The simple periodic structure supports a resonance which is symmetry forbidden to couple out of the structure to emit in the normal direction. It therefore, lends itself to smaller losses and larger quality factors. We calculate the electric fields and far-field distributions of modes supported in the periodic and quasi-aperiodic structures using the finite-difference time-domain (FDTD) method (Lumerical FDTD Solutions). The electric field intensity and in-plane electric field vectors of one such mode in the periodic array is illustrated in Figure 15c. Such modes are commonly referred to as uncoupled modes typically symmetry forbidden to couple to the continuum , and manifest themselves as donut or ring-like beams in the far-field as observed in Figure 15e. The short range aperiodicity in the quasi-aperiodic structure, however, breaks the mirror symmetry present in the original geometry thereby breaking the optical mode symmetry (Figure 15d), much like changing emitter shape in previous works[47-48]. Breaking the mirror symmetry reduces the resonance's Q and enables vertical light to escape more easily. Figure 15f in fact, shows a much more uniform emitted far-field distribution.

To compare with our theoretical predictions we measure the emitted far-field distributions of each resonance. The right inset of Figure 18 shows the measured far-field patterns produced by for both the periodic and quasi-aperiodic structures. As theoretically predicted, the higher Q simple periodic resonance (top right) emits a

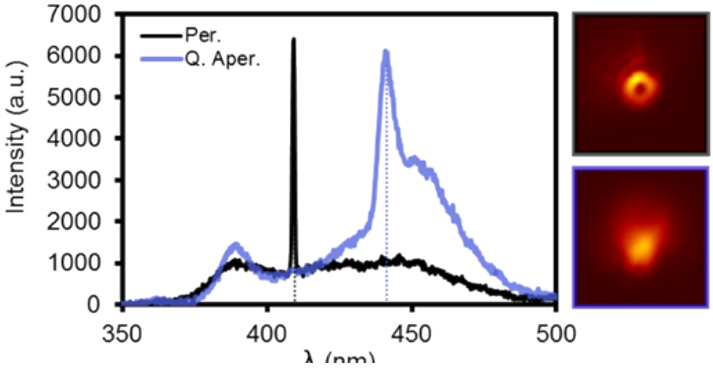

Figure 18. Room temperature PL for a simple periodic (black) and quasi-aperiodic (purple) device. Dashed lines indicate the center of a resonance in each device. (Right) Emitted far-field patterns for the simple periodic (top) and quasi-aperiodic (bottom) device.

donut-like beam while the lower Q, quasi-aperiodic resonance (bottom right) emits a more uniform beam. While donut beams can be vector beams possessing interesting polarization and angular momentum properties[49], they are not desirable beam profiles for lasing and lighting applications[47]. Using a quasi-aperiodic array, however, it is possible to significantly improve emission extraction in the normal direction and reshape the emitted beam profile.

To explore the possibility of lasing in such structures we studied evolution of the optical output intensity of the resonances as a function of input pump power for both cases (Figure 19a). For the simple periodic case, the output intensity of the resonance begins to linearly increase as the input power steadily increases. Near an input power density of 120 kW/cm^2, however, the input-output power relation turns strongly non-linear. For the quasi-aperiodic array (Figure 19b) the input power-output intensity remains linear up to an input of nearly 1200 kW/cm^2 before reaching the onset of non-

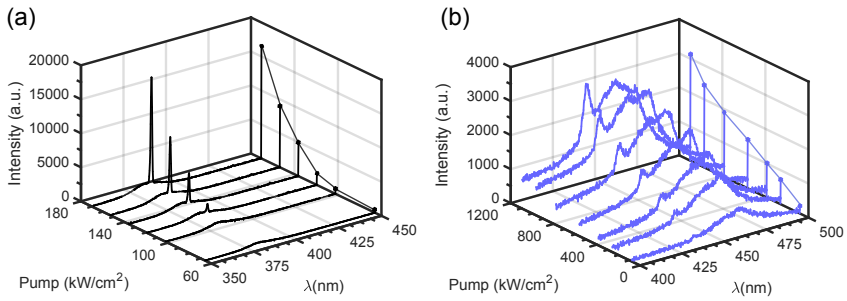

linearity.

Figure 19. Input-output power relations for a resonance in a (a) simple periodic array and (b) quasi-aperiodic array.

This onset requires nearly 10X more input power than the simple periodic device which is consistent with the 10X reduction in Q. Further increase of the input power resulted in a loss of the quasi-aperiodic resonance, likely due to optical damage. Theoretical Qs calculated using the finite-difference time domain (FDTD) method (Lumerical FDTD Solutions) predicted Qs of 442 and 129 for the simple periodic and the quasi-aperiodic arrays, respectively. While the theoretical Q for the simple periodic case is close to its measured value, the measured quasi-aperiodic Q is nearly 3X less than the theoretically calculated Q. This discrepancy likely arises from the close nanowire proximity in the quasi-aperiodic array and additional etch-plane competition during the KOH-based wet etch. The etch-plane competition effectively reduces the length of the nanowires, as evidenced from careful inspection of the nanowire bases (black arrows in Figure 5.3b). This reduction in nanowire height could potentially be mitigated using a two stage dry etch / wet etch process, but at the cost of increased fabrication complexity. Other possibilities for improving device performance include organic sulfide passivation, which has recently been shown to significantly improve the quantum efficiency of III-nitride nanowires. This work was accepted for publication in Optics materials express.

6. SUMMARY AND FUTURE

This work was motivated by the possiblility of III-nitride QDs as the active source for enhancing light emission for visible photonics such as LEDs and LDs. Modelling suggests that the gain onset for a QD based active region can occur about 100X lower carrier density as that of QWs. Furthermore higher spontaneous emission rate can also be achieved at higher carrier densities (stronger pump) for QD based LED versus QW. Finally higher power conversion efficiencies also onsets sooner for QD based LDs than for QW based LDs. These advantages not withstanding there are two main challenges that needs to be addressed for taking advantage of this phenomena: one, a robust technique for creating dense, monodisperse III-nitride QDs and two, optimize light coupling and light extraction from such QDs . To achieve the former we have utilized a recently developed QSC-PEC based top-down approach. This approach has demonstrated creation of QD arrays in MQWs however, many challenges still remain in creating a dense monodisperse dots. This approach also enables creation of single quantum dots which when combined with electron beam lithography patterning can enable deterministically placed single QDs which are important for single photon source. Finally, light extraction is also an important criteria for light sources and displays especially uniform far-field emission pattern. We have demonstrated that this can be achieved by utilizing a quasi-aperiodic array photonic crystal to break symmetry that enables better light coupling to the continuum. For the future the goal is to better understand the possibilities and limitations of achieve a dense quantum dot array from multiple quantum wells. Passivation techniques can be explored for potential reduction in internal quantum efficiencies of QDs during fabrication. An additional challenge is the integrated and monolithic design of the photonic crystal structures for emission manipulation that is electrically injected. If these issues can be successfully addressed there is a clear pathway for high efficiency large area photonic crystal lasers as well as photonic crystal based quantum sources.

.

REFERENCES

1. Hurni, C. A.; David, A.; Cich, M. J.; Aldaz, R. I.; Ellis, B.; Huang, K.; Tyagi, A.; DeLille, R. A.; Craven, M. D.; Steranka, F. M.; Krames, M. R., Bulk GaN flip-chip violet light-emitting diodes with optimized efficiency for high-power operation. *Applied Physics Letters* **2015,** *106* (3), 031101.
2. Tsao, J. Y.; Crawford, M. H.; Coltrin, M. E.; Fischer, A. J.; Koleske, D. D.; Subramania, G. S.; Wang, G. T.; Wierer, J. J.; Karlicek, R. F., Toward Smart and Ultra-efficient Solid-State Lighting. *Advanced Optical Materials* **2014,** *2* (9), 809-836.
3. Shen, Y. C.; Mueller, G. O.; Watanabe, S.; Gardner, N. F.; Munkholm, A.; Krames, M. R., Auger recombination in InGaN measured by photoluminescence. *Applied Physics Letters* **2007,** *91* (14), 141101.
4. Kioupakis, E.; Rinke, P.; Delaney, K. T.; Van de Walle, C. G., Indirect Auger recombination as a cause of efficiency droop in nitride light-emitting diodes. *Applied Physics Letters* **2011,** *98* (16), 161107.
5. David, A.; Grundmann, M. J., Influence of polarization fields on carrier lifetime and recombination rates in InGaN-based light-emitting diodes. *Applied Physics Letters* **2010,** *97* (3), 033501.
6. Iveland, J.; Martinelli, L.; Peretti, J.; Speck, J. S.; Weisbuch, C., Direct Measurement of Auger Electrons Emitted from a Semiconductor Light-Emitting Diode under Electrical Injection: Identification of the Dominant Mechanism for Efficiency Droop. *Phys. Rev. Lett.* **2013,** *110* (17), 177406.
7. Wierer, J. J.; Tsao, J. Y.; Sizov, D. S., Comparison between blue lasers and light-emitting diodes for future solid-state lighting. *Laser Photon. Rev.* **2013,** *7* (6), 963-993.
8. Wierer, J. J.; Tansu, N.; Fischer, A. J.; Tsao, J. Y., III-nitride quantum dots for ultra-efficient solid-state lighting. *Laser Photon. Rev.* **2016,** *10* (4), 612-622.
9. Li, Q.; Wright, J. B.; Chow, W. W.; Luk, T. S.; Brener, I.; Lester, L. F.; Wang, G. T., Single-mode GaN nanowire lasers. *Optics Express* **2012,** *20* (16), 17873-17879.
10. Li, Q.; Westlake, K. R.; Crawford, M. H.; Lee, S. R.; Koleske, D. D.; Figiel, J. J.; Cross, K. C.; Fathololoumi, S.; Mi, Z.; Wang, G. T., Optical performance of top-down fabricated InGaN/GaN nanorod light emitting diode arrays. *Optics Express* **2011,** *19* (25), 25528-25534.
11. Li, C.; Liu, S.; Luk, T. S.; Figiel, J. J.; Brener, I.; Brueck, S.; Wang, G. T., Intrinsic polarization control in rectangular GaN nanowire lasers. *Nanoscale* **2016,** *8* (10), 5682-5687.
12. Li, C.; Liu, S.; Hurtado, A.; Wright, J. B.; Xu, H.; Luk, T. S.; Figiel, J. J.; Brener, I.; Brueck, S. R.; Wang, G. T., Annular-Shaped Emission from Gallium Nitride Nanotube Lasers. *ACS Photonics* **2015,** *2* (8), 1025-1029.
13. Xiao, X.; Fischer, A. J.; Coltrin, M. E.; Lu, P.; Koleske, D. D.; Wang, G. T.; Polsky, R.; Tsao, J. Y., Photoelectrochemical etching of epitaxial InGaN thin films: self-limited kinetics and nanostructuring. *Electrochimica Acta* **2015,** *162*, 163-168.
14. Xiao, X.; Fischer, A. J.; Wang, G. T.; Lu, P.; Koleske, D. D.; Coltrin, M. E.; Wright, J. B.; Liu, S.; Brener, I.; Subramania, G. S., Quantum-Size-Controlled Photoelectrochemical Fabrication of Epitaxial InGaN Quantum Dots. *Nano Lett.* **2014,** *14* (10), 5616-5620.
15. Englund, D.; Fattal, D.; Waks, E.; Solomon, G.; Zhang, B.; Nakaoka, T.; Arakawa, Y.; Yamamoto, Y.; Vučković, J., Controlling the Spontaneous Emission Rate of Single Quantum Dots in a Two-Dimensional Photonic Crystal. *Phys. Rev. Lett.* **2005,** *95* (1), 013904.

16. Pelton, M.; Santori, C.; Vučković, J.; Zhang, B.; Solomon, G. S.; Plant, J.; Yamamoto, Y., Efficient Source of Single Photons: A Single Quantum Dot in a Micropost Microcavity. *Phys. Rev. Lett.* **2002,** *89* (23), 233602.
17. Gerard, J. M.; Gayral, B., Strong Purcell effect for InAs quantum boxes in three-dimensional solid-state microcavities. *Journal of Lightwave Technology* **1999,** *17* (11), 2089-2095.
18. Portalupi, S. L.; Hornecker, G.; Giesz, V.; Grange, T.; Lemaître, A.; Demory, J.; Sagnes, I.; Lanzillotti-Kimura, N. D.; Lanco, L.; Auffèves, A.; Senellart, P., Bright Phonon-Tuned Single-Photon Source. *Nano Lett.* **2015,** *15* (10), 6290-6294.
19. Buckley, S.; Rivoire, K.; Vučković, J., Engineered quantum dot single-photon sources. *Reports on Progress in Physics* **2012,** *75* (12), 126503.
20. Gallardo, E.; Martínez, L. J.; Nowak, A. K.; Sarkar, D.; Sanvitto, D.; van der Meulen, H. P.; Calleja, J. M.; Prieto, I.; Granados, D.; Taboada, A. G.; García, J. M.; Postigo, P. A., Single-photon emission by semiconductor quantum rings in a photonic crystal. *Journal of the Optical Society of America B* **2010,** *27* (6), A21-A24.
21. Michler, P.; Kiraz, A.; Becher, C.; Schoenfeld, W. V.; Petroff, P. M.; Zhang, L.; Hu, E.; Imamoglu, A., A Quantum Dot Single-Photon Turnstile Device. *Science* **2000,** *290* (5500), 2282.
22. Lounis, B.; Bechtel, H. A.; Gerion, D.; Alivisatos, P.; Moerner, W. E., Photon antibunching in single CdSe/ZnS quantum dot fluorescence. *Chemical Physics Letters* **2000,** *329* (5), 399-404.
23. Rossetti, R.; Ellison, J. L.; Gibson, J. M.; Brus, L. E., Size effects in the excited electronic states of small colloidal CdS crystallites. *The Journal of Chemical Physics* **1984,** *80* (9), 4464-4469.
24. Labeau, O.; Tamarat, P.; Lounis, B., Temperature Dependence of the Luminescence Lifetime of Single CdSe/ZnS Quantum Dots. *Phys. Rev. Lett.* **2003,** *90* (25), 257404.
25. Matsumoto, H.; Sakata, T.; Mori, H.; Yoneyama, H., Preparation of Monodisperse CdS Nanocrystals by Size Selective Photocorrosion. *The Journal of Physical Chemistry* **1996,** *100* (32), 13781-13785.
26. Deshpande, S.; Frost, T.; Yan, L.; Jahangir, S.; Hazari, A.; Liu, X.; Mirecki-Millunchick, J.; Mi, Z.; Bhattacharya, P., Formation and Nature of InGaN Quantum Dots in GaN Nanowires. *Nano Lett.* **2015,** *15* (3), 1647-1653.
27. Nguyen, H. P. T.; Cui, K.; Zhang, S.; Fathololoumi, S.; Mi, Z., Full-color InGaN/GaN dot-in-a-wire light emitting diodes on silicon. *Nanotechnology* **2011,** *22* (44), 445202.
28. Hatami, F.; Masselink, W. T.; Schrottke, L.; Tomm, J. W.; Talalaev, V.; Kristukat, C.; Goñi, A. R., InP quantum dots embedded in GaP: Optical properties and carrier dynamics. *Physical Review B* **2003,** *67* (8), 085306.
29. Marzin, J. Y.; Gérard, J. M.; Izraël, A.; Barrier, D.; Bastard, G., Photoluminescence of Single InAs Quantum Dots Obtained by Self-Organized Growth on GaAs. *Phys. Rev. Lett.* **1994,** *73* (5), 716-719.
30. Frank, F. C.; van der Merwe, J. H., One-Dimensional Dislocations. I. Static Theory. *Proceedings of the Royal Society of London. Series A. Mathematical and Physical Sciences* **1949,** *198* (1053), 205.
31. Grandjean, N.; Ilegems, M., Visible InGaN/GaN Quantum-Dot Materials and Devices. *Proceedings of the IEEE* **2007,** *95* (9), 1853-1865.

32. Ropp, C.; Cummins, Z.; Nah, S.; Fourkas, J. T.; Shapiro, B.; Waks, E., Nanoscale imaging and spontaneous emission control with a single nano-positioned quantum dot. *Nat Commun* **2013,** *4*, 1447.
33. Ropp, C.; Cummins, Z.; Probst, R.; Qin, S.; Fourkas, J. T.; Shapiro, B.; Waks, E., Positioning and Immobilization of Individual Quantum Dots with Nanoscale Precision. *Nano Lett.* **2010,** *10* (11), 4673-4679.
34. Thon, S. M.; Rakher, M. T.; Kim, H.; Gudat, J.; Irvine, W. T. M.; Petroff, P. M.; Bouwmeester, D., Strong coupling through optical positioning of a quantum dot in a photonic crystal cavity. *Applied Physics Letters* **2009,** *94* (11), 111115.
35. Fischer, A. J.; Anderson, P. D.; Koleske, D. D.; Subramania, G., Deterministic Placement of Quantum-Size Controlled Quantum Dots for Seamless Top-Down Integration. *ACS Photonics* **2017**.
36. Wright, J. B.; Liu, S.; Wang, G. T.; Li, Q.; Benz, A.; Koleske, D. D.; Lu, P.; Xu, H.; Lester, L.; Luk, T. S.; Brener, I.; Subramania, G., Multi-Colour Nanowire Photonic Crystal Laser Pixels. *Sci. Rep.* **2013,** *3*, 2982.
37. Shusuke, I.; Katsumi, K.; Ryuichi, A.; Akihiko, K.; Shuichi, S., Optically Pumped Green (530–560 nm) Stimulated Emissions from InGaN/GaN Multiple-Quantum-Well Triangular-Lattice Nanocolumn Arrays. *Appl. Phys. Express* **2011,** *4* (5), 055001.
38. Scofield, A. C.; Kim, S.-H.; Shapiro, J. N.; Lin, A.; Liang, B.; Scherer, A.; Huffaker, D. L., Bottom-up Photonic Crystal Lasers. *Nano Lett.* **2011,** *11* (12), 5387-5390.
39. Diedenhofen, S. L.; Janssen, O. T. A.; Hocevar, M.; Pierret, A.; Bakkers, E. P. A. M.; Urbach, H. P.; Gómez Rivas, J., Controlling the Directional Emission of Light by Periodic Arrays of Heterostructured Semiconductor Nanowires. *ACS Nano* **2011,** *5* (7), 5830-5837.
40. Wiesmann, C.; Bergenek, K.; Linder, N.; Schwarz, U., Photonic crystal LEDs - designing light extraction. *Laser Photon. Rev.* **2009,** *3* (3), 262-286.
41. Wierer, J. J.; David, A.; Megens, M. M., III-nitride photonic-crystal light-emitting diodes with high extraction efficiency. *Nat Photon* **2009,** *3* (3), 163-169.
42. David, A.; Benisty, H.; Weisbuch, C., Spontaneous emission in GaN/InGaN photonic crystal nanopillars. *Optics Express* **2007,** *15* (26), 17991-18004.
43. Fujita, M.; Takahashi, S.; Tanaka, Y.; Asano, T.; Noda, S., Simultaneous Inhibition and Redistribution of Spontaneous Light Emission in Photonic Crystals. *Science* **2005,** *308* (5726), 1296-1298.
44. Lee, R. K.; Xu, Y.; Yariv, A., Modified spontaneous emission from a two-dimensional photonic bandgap crystal slab. *J. Opt. Soc. Am. B* **2000,** *17* (8), 1438-1442.
45. Fan, S.; Villeneuve, P. R.; Joannopoulos, J. D.; Schubert, E. F., High Extraction Efficiency of Spontaneous Emission from Slabs of Photonic Crystals. *Phys. Rev. Lett.* **1997,** *78* (17), 3294.
46. Anderson, P. D.; Povinelli, M. L., Optimized emission in nanorod arrays through quasi-aperiodic inverse design. *Optics Letters* **2015,** *40* (11), 2672-2675.
47. Hirose, K.; Liang, Y.; Kurosaka, Y.; Watanabe, A.; Sugiyama, T.; Noda, S., Watt-class high-power, high-beam-quality photonic-crystal lasers. *Nat Photon* **2014,** *8* (5), 406-411.
48. Miyai, E.; Sakai, K.; Okano, T.; Kunishi, W.; Ohnishi, D.; Noda, S., Photonics: Lasers producing tailored beams. *Nature* **2006,** *441* (7096), 946-946.
49. Franke-Arnold, S.; Allen, L.; Padgett, M., Advances in optical angular momentum. *Laser Photon. Rev.* **2008,** *2* (4), 299-313.

[Blank page following section.]

APPENDIX A: LIST OF PUBLICATIONS AND PRESENTATIONS

Publications (published, in preparation or review)

1. Wierer, J. J., Tansu, N., Fischer, A. J. & Tsao, J. Y. III-nitride quantum dots for ultra-efficient solid-state lighting. Laser Photon. Rev. 10, 612-622, doi:10.1002/lpor.201500332 (2016).

2. Subramania, G.; Fischer, A. J.; Anderson, P. D.; Koleske, D. D. In Deterministically placed quantum dots for quantum nanophotonics, 2016 18th International Conference on Transparent Optical Networks (ICTON), 10-14 July 2016; 2016; pp 1-4.

3. A.J. Fischer, P.D. Anderson, D. D. Koleske, G. Subramania, "Deterministic Placement of Quantum-Size Controlled Quantum Dots for Seamless Top-Down Integration", accepted in ACS Photonics (2017). DOI: 10.1021/acsphotonics.7b00774

4. P.D. Anderson, D. D. Koleske, M. Povinelli, G. Subramania, "Tailoring emission uniformity and band dispersion in nanowire arrays using quasi-aperiodic design", accepted in Optics Materials Express.

Patents

1. Jonathan Wierer, JR., Jeffrey Y. Tsao, Arthur J. Fischer,"White light illuminant comprising quantum dot lasers and phosphors", US 20160087406 A1.

Presentations

- 16 invited presentations/seminars
    - G.T. Wang (10), A.J. Fischer(2), G. Subramania(4)]

Professional leadership and recognition

- G. Subramania , Organizing chair of Active Photonics Materials conference at SPIE Optics & Photonics, San Diego, CA.

DISTRIBUTION

4 Lawrence Livermore National Laboratory
Attn: N. Dunipace (1)
P.O. Box 808, MS L-795
Livermore, CA 94551-0808

1	MSXXXX	Name of Person	Org. Number
1	MSXXXX	Name of Person	Org. Number

[The housekeeping entries are required for all SAND reports.]

1	MS0899	Technical Library	9536 (electronic copy)

For LDRD reports, add:

1	MS0359	D. Chavez, LDRD Office	1911

For CRADA reports add:

1	MS0115	OFA/NFE Agreements	10012

For Patent Caution reports, add:

1	MS0161	Legal Technology Transfer Center	11500


Sandia National Laboratories